ADVANCED FUNCTIONAL MATERIALS
www.afm-journal.de

Smart Supramolecular "Trojan Horse"-Inspired Nanogels for Realizing Light-Triggered Nuclear Drug Influx in Drug-Resistant Cancer Cells

Xiaokai Chen, Xiaodong Zhang, Yuxin Guo, Ya-Xuan Zhu, Xiaoyang Liu, Zhan Chen, and Fu-Gen Wu**

Efficient nuclear delivery of anticancer drugs evading drug efflux transporters (DETs) on the plasma and nuclear membranes of multidrug-resistant cancer cells is highly challenging. Here, smart nanogels are designed via a one-step self-assembly of three functional components including a biocompatible copolymer, a fluorescent organosilica nanodot, and a photodegradable near-infrared (NIR) dye indocyanine green (ICG). The rationally designed nanogels have high drug encapsulation efficiency (≈99%) for anticancer drug doxorubicin (Dox), self-traceability for bioimaging, proper size for passive tumor targeting, prolonged blood circulation time for enhanced drug accumulation in tumor, and photocontrolled disassemblability. Moreover, the Dox-loaded nanogels can effectively kill multidrug-resistant cells via two steps: 1) They behave like a "Trojan horse" to escape from the DETs on the plasma membrane for efficiently transporting the anticancer "soldier" (Dox) into the cytoplasm and preventing the drugs from being excreted from the cells; 2) Upon NIR light irradiation, the photodegradation of ICG leads to the disassembly of the nanogels to release massive Dox molecules, which can evade the DETs on the nuclear membrane to exert their intranuclear efficacy in multidrug-resistant cells. Combined with their excellent biocompatibility, the nanogels may provide an alternative solution for overcoming cancer multidrug resistance.

1. Introduction

Multidrug resistance (MDR) leading to the insufficient intracellular and intranuclear accumulation of anticancer drugs is a major obstacle to the success of cancer chemotherapy. Overcoming MDR has become an urgent issue for the development of effective cancer therapeutic strategies. Overexpression of the drug efflux transporters (DETs), e.g., P-glycoprotein (P-gp), is considered as the major mechanism causing MDR; meanwhile, overexpressed or activated anti-apoptosis proteins help cancer cells to escape from apoptosis.[1] In recent years, nanocarriers have attracted much attention in combating cancer MDR due to their capability to bypass the P-gp-mediated drug efflux,[2] since the efflux channel of P-gp only allows for the passage of small molecules (300–2000 Da).[1b] To further improve the therapeutic effect, several measures have been adopted to reverse MDR, including 1) the use of corresponding inhibitors to suppress DET function,[3] 2) the approach to weaken the function of anti-apoptosis proteins and to induce paraptosis,[4] 3) the strategy to knock down the expression of the genes related to drug resistance based on ribonucleic acid (RNA) interference technology,[1d,5] 4) the assistance of magnetic field to target and kill multidrug-resistant cells,[6] and 5) the employment of pH-, reduction-, or hyperthermia-responsiveness for drug release and tumor penetration.[7] Although most of these therapeutic methods can enhance the intracellular uptake of drugs, their therapeutic performance is still unsatisfactory because of the low drug accumulation in cell nucleus which is the ultimate target of most chemotherapeutics including doxorubicin (Dox), cisplatin, and camptothecin (CPT).[1b,8] Besides, the above therapeutic methods are usually encountered by one or some of the following drawbacks including high cost, complicated synthetic procedures, poor controllability of drug release, inaccurate targeting to multidrug-resistant cells, and potential injury to normal issues. Although a few reports have adopted small nanoparticles (NPs; ≤8 nm) to directly transport drugs across nuclear envelope to combat MDR,[9] such a strategy still suffers from insufficient intracellular and intranuclear accumulation due to the reduced circulation life of small nanoparticles. Furthermore, it should be noted that due to the presence of DETs on the nuclear membrane,[10]

X. K. Chen, X. D. Zhang, Y. X. Guo, Y.-X. Zhu, X. Y. Liu, Prof. F.-G. Wu
State Key Laboratory of Bioelectronics
School of Biological Science and Medical Engineering
Southeast University
2 Sipailou Road, Nanjing 210096, P. R. China
E-mail: wufg@seu.edu.cn
Prof. Z. Chen
Department of Chemistry
University of Michigan
930 North University Avenue, Ann Arbor, MI 48109, USA
E-mail: zhanc@umich.edu
The ORCID identification number(s) for the author(s) of this article can be found under https://doi.org/10.1002/adfm.201807772.

DOI: 10.1002/adfm.201807772

few anticancer drugs that take effect in cell nucleus can pass through the nuclear membrane, resulting in the failure of the circumvention of cancer MDR.

On the other hand, nanogels as nanosized crosslinked polymer networks, which combine the properties of both hydrogels and nanomaterials, have attracted great interest due to their excellent properties such as high water contents, tunable chemical and physical structures, large surface areas for bioconjugation, long blood circulation time, excellent tumor-targeting performance, and good biocompatibility.[11] In recent years, nanogels have been widely applied as drug delivery systems,[12] imaging and sensing agents,[13] and theranostic materials.[14] Herein, inspired by the design of "Trojan horse," we rationally developed photocontrollable nanogels (denoted as SiPINGs) via simple supramolecular self-assembly of three functional components: biocompatible methoxypoly(ethylene glycol)5*k*-*block*-poly(*L*-glutamic acid sodium salt)$_{200}$ (PEG–PLE), green fluorescent organosilica nanodot (OSiND), and photodegradable indocyanine green (ICG). The as-formed self-traceable SiPINGs play a role of the "Trojan horse" and show great potential as a multifunctional nanoplatform to effectively overcome MDR based on the following two-step approach: First, the anticancer "soldier" (Dox) itself is difficult to cross the plasma membrane which acts as the gate of cells due to the presence of the DETs. By hiding inside the "Trojan horse"-like nanogels with appropriate surface coating (PEG–PLE) to escape from the recognition by DETs, a large number of the "soldiers" (Dox molecules) are transported into the multidrug-resistant cells via caveolin-, clathrin-, and macropinocytosis-mediated endocytosis pathways. The numerous "soldiers" are widely distributed in the cytoplasm contributing to a high local concentration near cell nucleus, serving as a prerequisite for further delivering them into the cell nucleus. Second, taking advantage of the phototriggered disassembly of the nanogels, massive "soldiers" are released from the nanogels to the cytoplasm, and then rapidly occupy the nucleus even in the presence of DETs on the nuclear membrane, thus realizing effective circumvention of MDR (**Scheme 1**). Overall, combined with the significantly improved hemocompatibility and biocompatibility of Dox@SiPINGs, we successfully developed a facile method to prepare a robust nanogel-based theranostic agent, which will offer a new opportunity to combat cancer MDR.

2. Results and Discussion

The photocontrollable "Trojan horse"-inspired SiPINGs (**Figure 1**a) with anti-MDR ability were prepared by a simple mixing of three functional materials including a biodegradable polymer (PEG–PLE) for surface coating to evade the recognition of DETs,[15] a green-emitting OSiND (synthesized according to our previous work[16]) for self-traceability, and a photodegradable cyanine dye ICG for photocontrollable drug release. To achieve efficient tumor accumulation via the enhanced permeability and retention (EPR) effect and bypass the efflux pump of multidrug-resistant cells, the nanoparticle sizes should be in the range of 20–250 nm.[1b,2g] Consequently, the weight ratio of PEG–PLE:OSiNDs:ICG was optimized to be 1:5:0.5. Transmission electron microscopy (TEM) images (Figure 1b and Figure S1a, Supporting Information) collected at low and high magnifications and the corresponding size distribution histogram (Figure 1c) showed a spherical structure of SiPINGs with an average diameter of ≈39.3 nm, which is smaller than their average hydrodynamic size (≈54.2 nm, measured by dynamic light scattering (DLS) due to the presence of a hydration layer of the nanogel (Figure S1b, Supporting Information)). Notably, many nanodots (similar to the OSiNDs in the TEM image of Figure S2, Supporting Information) can be observed within the spheroid (Figure 1b, marked by white arrows), suggesting the important role of OSiNDs (amine-rich) as a bridge between PEG–PLE (negatively charged) and ICG (negatively charged) molecules to promote the formation of SiPINGs. SiPINGs had a surface potential of −39.1 ± 3.8 mV (Figure S3, Supporting

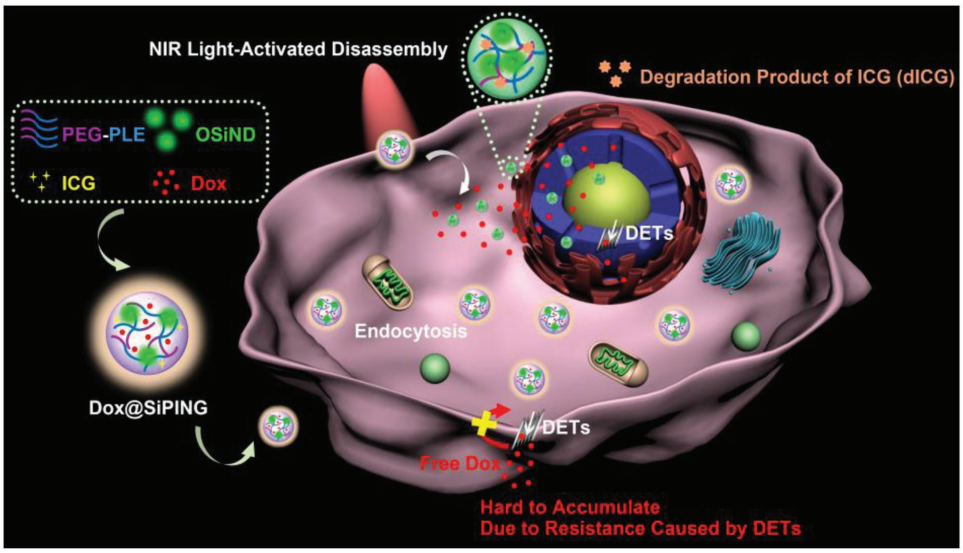

Scheme 1. Schematic illustrating the rational design of Dox-encapsulated nanogels that behave like "Trojan horses" for enhancing cellular uptake and nuclear delivery of drugs to circumvent cancer MDR.

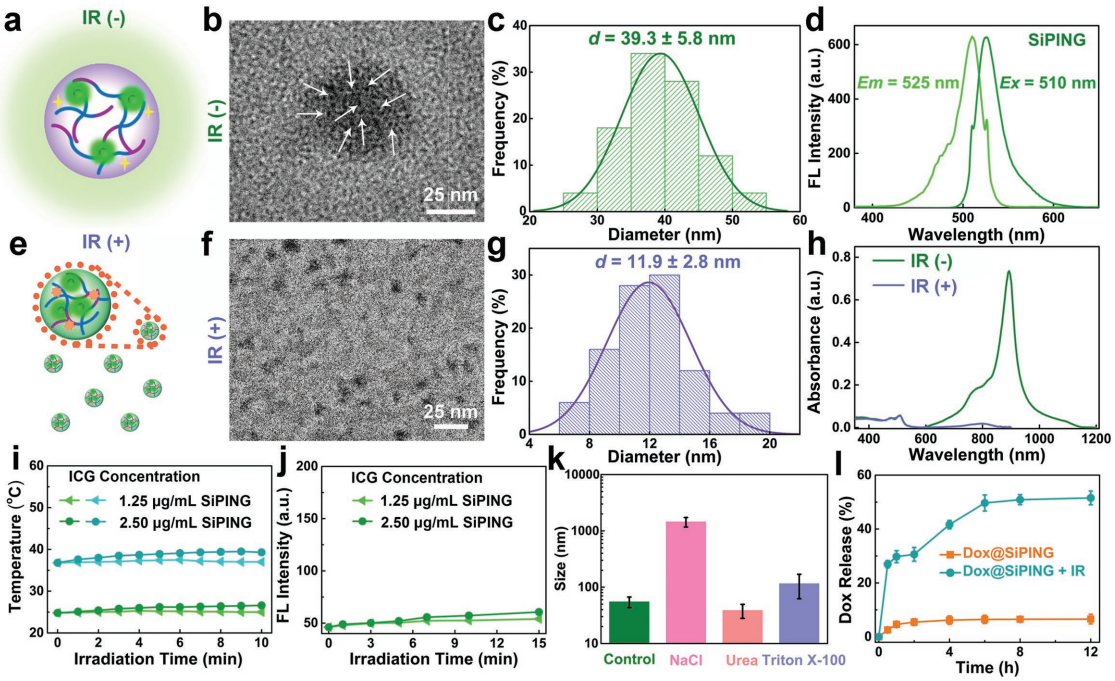

Figure 1. a) Schematic illustration, b) TEM image (obtained at a high magnification), c) corresponding size distribution histogram, and d) fluorescence excitation and emission spectra of SiPING suspension before irradiation (IR). e) Schematic illustration, f) TEM image, and g) corresponding size distribution histogram of SiPINGs after irradiation. h) Absorption spectra of SiPING suspension before and after irradiation (808 nm, 0.5 W cm^{-2}, 10 min). i) Temperature change curves of SiPING suspension under an 808 nm laser irradiation for 10 min (the environment temperature was 25 or 37 °C). j) Singlet oxygen production of SiPING suspension under an 808 nm laser irradiation for up to 15 min. k) Hydrodynamic sizes of the self-assemblies formed by PEG–PLE, OSiNDs, ICG, and one of the three inhibitors (NaCl, urea, or Triton X-100; at a concentration of 0.2 M). l) Dox release profiles from Dox@SiPINGs with and without irradiation (808 nm, 0.5 W cm^{-2}, 10 min).

Information), suggesting that the negatively charged PEG–PLE and ICG were on the surface of the nanogels. Meanwhile, it was found that the fluorescence (FL) properties of the green-emitting OSiNDs were not affected after the nanogel formation (Figure 1d and Figure S4, Supporting Information).

To demonstrate the photocontrollability of the nanogels, the SiPING suspension was irradiated by an 808 nm laser (0.5 W cm^{-2}, 10 min). The nanogels were disassembled (Figure 1e) into many small nanoparticles (Figure 1f) with a much smaller average diameter of ≈11.9 nm (Figure 1g), which are similar to the assemblies of the three components including PEG–PLE, OSiNDs, and the degradation product of ICG (dICG) (Figure S5a,b, Supporting Information). In contrast, the assemblies of "PEG–PLE + OSiNDs," "PEG–PLE + dICG," and "OSiNDs + dICG" (Figure S5c–e, Supporting Information) had much larger sizes than the abovementioned small nanoparticles. Further, to investigate the formation mechanism of the small nanoparticles, NaCl, urea, and Triton X-100 were adopted to exert electrostatic shielding effect, destroy the hydrogen bonds, and disassociate the hydrophobic interaction, respectively. From the changes of hydrodynamic diameters as revealed by DLS (Figure S5f, Supporting Information), the formation mechanism of the assemblies was mainly attributed to the electrostatic and hydrophobic interactions. Meanwhile, the photoactivated disassembly of the nanogels was also confirmed in the absorption spectra. ICG had a strong absorption peak at ≈780 nm (Figure S6a, Supporting Information), while the peak of SiPINGs red-shifted to ≈880 nm (Figure 1h), indicating the aggregation of ICG molecules within the nanogel. After near-infrared (NIR) light irradiation (808 nm, 0.5 W cm^{-2}, 10 min), the peak of SiPINGs in the NIR region moved to ≈800 nm, and its intensity remarkably decreased. On the other hand, the matrix-assisted laser desorption/ionization time-of-flight (MALDI-TOF) mass spectrometry experiments were performed. Free ICG showed a strongest peak at ≈753 (Figure S6b, Supporting Information), while the dICG had several peaks in the region of m/z = 200–800 (Figure S6c, Supporting Information), which can be assigned to the corresponding degraded products as shown in Figure S6d in the Supporting Information. The absorption spectroscopic data and MALDI-TOF mass spectrometric results confirmed the photodegradation of ICG under NIR laser irradiation, which led to the disassembly of SiPINGs. Besides, a negligible increase in the temperature (Figure 1i) and a negligible production of single oxygen (Figure 1j) were detected when the SiPING suspension (with the same concentrations as those used in the following in vitro experiments) was under irradiation, which eliminated the possibility of photothermal (PT) and photodynamic (PD) effects and ensured the biosafety of the nanogels without side effects caused by PT or PD effect.

Next, the formation mechanism of the nanogels was also investigated. The DLS results showed that the addition of NaCl had a strong effect on the hydrodynamic diameter of the nanogels, while the addition of urea and Triton X-100 also had influence on the hydrodynamic diameters (Figure 1k),

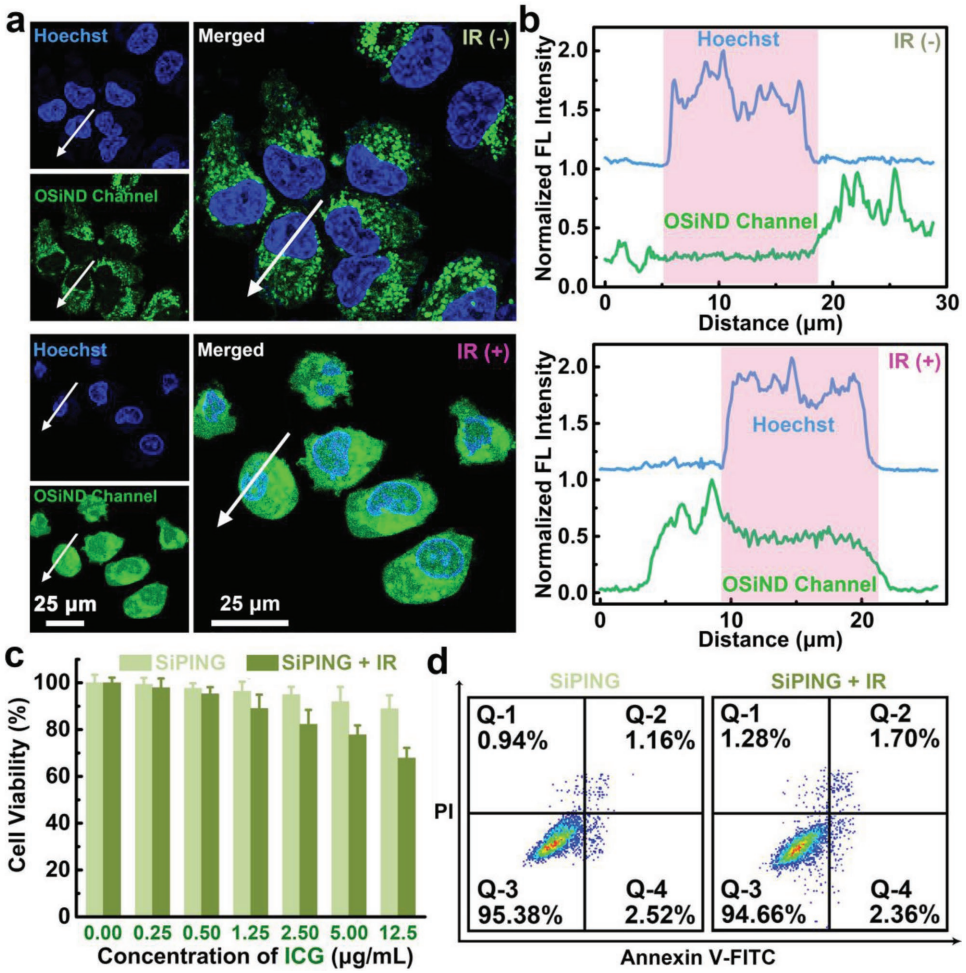

Figure 2. a) Confocal fluorescence images of SiPINGs-treated MCF-7/ADR cells before and after NIR light irradiation. The cell nuclei were stained with Hoechst 33342 (abbreviated as Hoechst). b) Normalized line-scan FL intensity profiles of the marked positions (white arrows in (a)). c) Cytotoxicity evaluation results of MCF-7/ADR cells treated with different ICG concentrations of SiPINGs or SiPINGs + irradiation (808 nm, 0.5 W cm^{-2}, 10 min). d) Apoptosis assay results of MCF-7/ADR cells with the treatment of SiPINGs or SiPINGs + IR (808 nm, 0.5 W cm^{-2}, 10 min). The ICG concentration of SiPINGs was 1.25 μg mL^{-1}.

indicating that the nanogel formation was mainly due to the electrostatic interaction, accompanied by some contributions from the hydrogen bonding and hydrophobic interaction. Additionally, to verify the indispensability of the three components (PEG–PLE, OSiNDs, and ICG) in forming the nanogels, the photographs and DLS results of the mixtures from various combinations of the three components were collected (Figure S7, Supporting Information). Although the mixture of PEG–PLE and OSiNDs was able to form nanogels (named as PSiNGs) with a hydrodynamic diameter of ≈58.5 nm (Figure S7b, Supporting Information), the absence of ICG made the nanogels unable to release the cargoes (such as Dox) in a photocontrollable way. Besides, many aggregates could be seen in the mixture containing OSiNDs and ICG (Figure S7a, Supporting Information), and large particles (>300 nm) were produced in the mixture of PEG–PLE and ICG (Figure S7c, Supporting Information), demonstrating the essential functions of PEG–PLE and OSiNDs in improving the water dispersibility and tuning the size of the nanogels, respectively. Collectively, the above results confirmed that all the three components are indispensable in forming the nanogels with suitable size, excellent water dispersibility, appropriate surface coating, and light-controllable drug release capability.

Motivated by the above results, we next tested the feasibility of using the photocontrollable nanogels to overcome cancer MDR in vitro. Since the drug efflux of multidrug-resistant cells is a main cause limiting the efficacy of chemotherapeutics, we investigated the cellular uptake and intracellular distribution of the nanogels in MCF-7 (a human breast cancer cell line) and adriamycin-resistant MCF-7 (MCF-7/ADR, a multidrug-resistant human breast cancer cell line) cells. Using the traceability of OSiNDs, significant accumulation of SiPINGs was observed in both MCF-7 and MCF-7/ADR cells (**Figure 2**a and Figure S8a, Supporting Information), showing that the "Trojan horse"-inspired nanogels could efficiently bypass the drug efflux pumps of multidrug-resistant cells with their proper size (≈39 nm, Figure 1c) and appropriate surface coating (PEG–PLE).

The fluorescence signals of SiPINGs were widely distributed in cytoplasm near cell nuclei due to the small size of nuclear pores (9–12 nm[17]). Interestingly, apparent intranuclear fluorescence signals were detected for both MCF-7 (Figure S8a,b, Supporting Information) and MCF-7/ADR (Figure 2a,b) cells after NIR light exposure, demonstrating the disassembly of nanogels and the subsequent nuclear entry of small particles (≈11.9 nm in Figure 1g). The above results suggested that SiPINGs could behave as a platform to effectively deliver small molecule drugs into cell nuclei.

To explore the cellular uptake mechanism of SiPINGs, the endocytosis pathways of the nanogels were studied. Sodium azide and the 4 °C treatment were adopted to investigate the influence of energy since endocytosis is an energy-dependent transport process.[18] In addition, different inhibitors including chlorpromazine (CPZ), genistein, and amiloride were used to inhibit clathrin-, caveolae-, and macropinocytosis-mediated pathways, respectively.[16] The flow cytometric results indicated that the internalization of SiPINGs was significantly inhibited by genistein, CPZ, amiloride, sodium azide, and 4 °C treatment (Figure S9, Supporting Information), revealing the caveolin-, clathrin-, and macropinocytosis-mediated endocytosis. Meanwhile, SiPINGs presented favorable biocompatibility with low dark- and photo-toxicities detected by 3-(4,5-dimethyl-2-thiazolyl)-2,5-diphenyl-2-*H*-tetrazolium bromide (MTT) and flow cytometry-based apoptosis assays (Figure 2c,d; Figure S8c,d and Table S1, Supporting Information), which can be credited to the biocompatible components (including PEG–PLE,[19] silicon-containing nanomaterials,[20] and United States Food and Drug Administration (FDA)-approved ICG[21]) and the very low content of ICG (which could not cause a significant temperature increase in the cells). The results also suggested that the high intracellular local concentration of ICG had negligible influence on the cell viability. To elucidate whether the combination treatment of SiPINGs and NIR light irradiation could affect the MCF-7/ADR cells, propidium iodide (PI), which can be used as a fluorescent nuclear stain to assess membrane integrity,[22] was used. Flow cytometric results showed that the fluorescence intensity of PI in the cells treated with SiPINGs + irradiation (IR) was similar to that in the cells treated with SiPINGs alone (Figure S10, Supporting Information), indicating that NIR light irradiation caused negligible influence on the integrity/permeability of the plasma membranes in the SiPING-treated cells. Taken together, the "Trojan horse"-inspired nanogels with efficient nuclear delivery of drugs exhibit great potential as an effective nanoplatform to fully overcome the cancer cell drug resistance.

Encouraged by the successful synthesis of photocontrollable SiPINGs with effective nuclear delivery, Dox, an anticancer agent on the World Health Organization's List of Essential Medicines,[23] was encapsulated into the nanogels (termed as Dox@SiPINGs, Figure S11a, Supporting Information). The TEM images (Figure S11b and Figure S1c, Supporting Information) and DLS result (Figure S1d, Supporting Information) of Dox@SiPINGs were similar to those of SiPINGs (Figure 1b,c and Figure S1a,b, Supporting Information). Importantly, the nanoagents exhibited an ultrahigh Dox encapsulation efficiency of ≈99% and loading efficiency of ≈23.5%. The fluorescence intensities of Dox, OSiNDs, and ICG in Dox@SiPINGs decreased to ≈30%, ≈70%, and ≈30%, respectively, compared to those of free Dox, OSiNDs, and ICG (Figure S12, Supporting Information), indicating the strong interaction among Dox, OSiNDs, and ICG. Nevertheless, Dox@SiPINGs still emitted strong green fluorescence (Figure S11c and Figure S12a, Supporting Information) due to the ultrahigh quantum yield of OSiNDs, ensuring their self-traceable ability. Besides, owing to their negatively charged surface with zeta potential of -34.6 ± 4.2 mV (Figure S3, Supporting Information) and PEG coating, the Dox-encapsulated nanogels displayed good stability without forming protein corona in fetal bovine serum (FBS)-containing cell medium, as proved by the DLS results (Figure S13 and Figure S1d, Supporting Information). With the characteristic of NIR light-triggerable disassembly (Figure S11d, Supporting Information), the size of Dox@SiPINGs changed from ≈40 to ≈10 nm after irradiation (Figure S11e, Supporting Information); meanwhile, the absorbance in the region >700 nm was markedly reduced, accompanied with a blue shift of the peak position (Figure S11f, Supporting Information). Afterward, sustained and efficient drug release of Dox@SiPINGs via the NIR light-controllable strategy was exhibited by the rapidly increased Dox concentration within 30 min and a final Dox release rate of ≈52% after irradiation (the cyan line in Figure 1l). Notably, the nanogels also presented excellent Dox leakage resistance in the absence of irradiation (the orange line in Figure 1l), minimizing their dark toxicity during their in vitro and in vivo applications.

As a proof of concept, we compared the endocytosis and anticancer performance of free Dox and Dox-encapsulated nanogels (Dox@SiPINGs) in MCF-7 and MCF-7/ADR cells. Confocal images showed that the accumulation of free Dox in MCF-7 cells was high after 6 h of incubation (Figure S14a,b, Supporting Information), while the red fluorescence signals of free Dox in MCF-7/ADR cells could hardly be detected during the whole time period of 24 h due to the high expression of DETs in MCF-7/ADR cells (**Figure 3**a,b). By contrast, significant uptake of Dox@SiPINGs was observed in MCF-7 and MCF-7/ADR cells within 3 h (Figure 3a and Figure S14a, Supporting Information), showing the strong capability of the nanogels to bypass the drug efflux pumps on the plasma membranes of the two types of cancer cells. Meanwhile, the long-time (at least 24 h) stable accumulation in the cytoplasm with negligible nucleus distribution demonstrated the good leakage resistance of Dox@SiPINGs, which ensured a sufficient Dox concentration for further sustained release of the drugs into cell nuclei upon NIR light irradiation. Besides, the bright yellow color in the cytoplasm of MCF-7 and MCF-7/ADR cells (Figures S15 and S16, Supporting Information) exhibited the excellent colocalization of green-emitting OSiNDs and red fluorescent Dox, further confirming the intracellular stability of the drug-loaded nanocarriers. Furthermore, from the effects of genistein, CPZ, amiloride, sodium azide, and 4 °C treatments on the internalization of Dox@SiPINGs (Figure S17, Supporting Information), we revealed a caveolin-, clathrin-, and macropinocytosis-mediated endocytosis pathway that might contribute to the high cellular internalization of Dox@SiPINGs in MCF-7/ADR cells. Nevertheless, sodium azide (NaN_3) could negligibly affect the cellular uptake of free Dox (Figure S18, Supporting Information), because Dox enters cells via an energy-independent free diffusion process.[24]

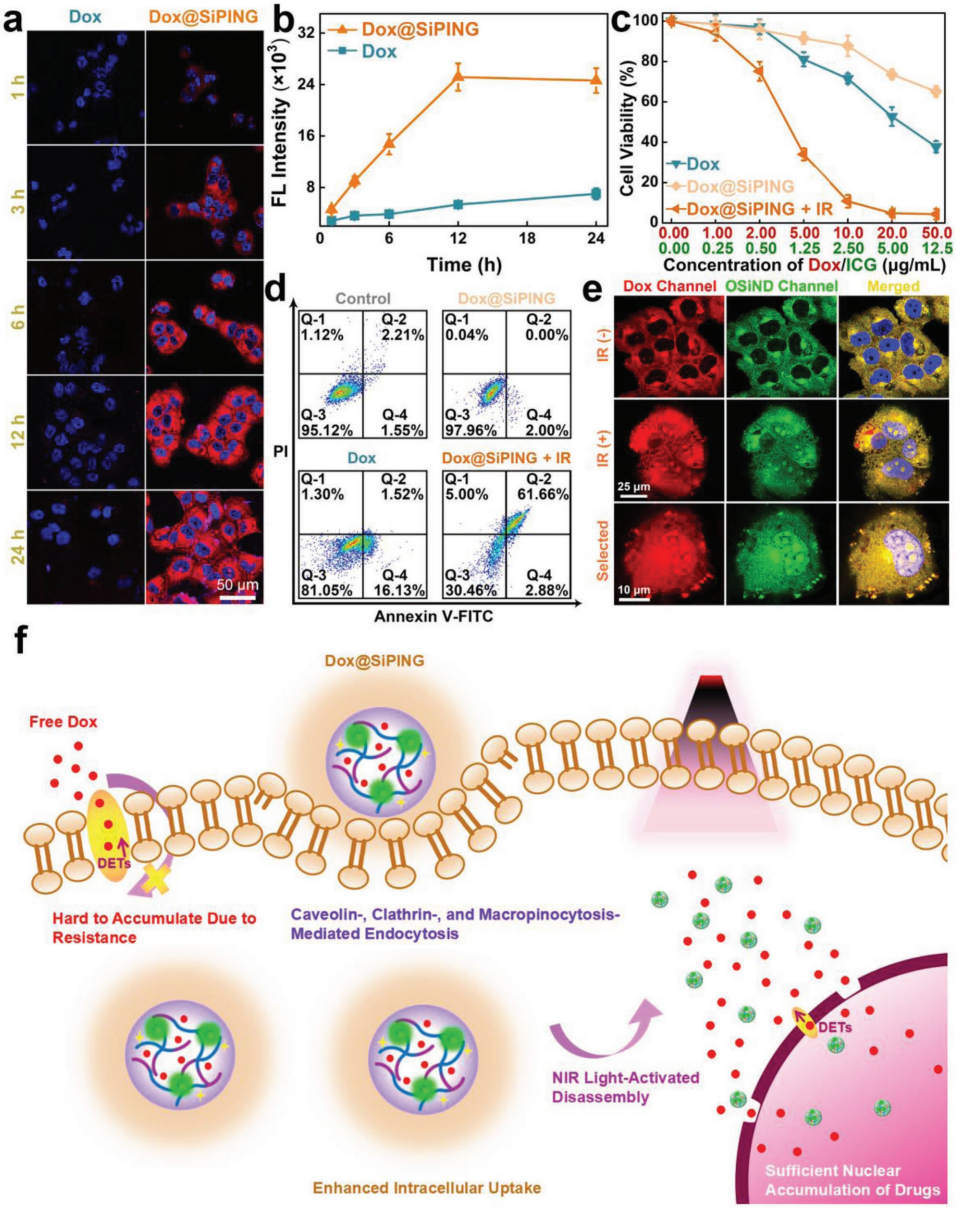

Figure 3. a) Confocal fluorescence images of MCF-7/ADR cells treated with the Dox or Dox@SiPINGs for different time periods, and b) the corresponding flow cytometric results. c) Cytotoxicity evaluation results of MCF-7/ADR cells after various treatments. d) Apoptosis assay results of MCF-7/ADR cells without and with the treatment of Dox, Dox@SiPINGs, or Dox@SiPINGs + IR (808 nm, 0.5 W cm^{-2}, 10 min) at the Dox concentration of 5.0 μg mL^{-1}. e) Confocal fluorescence images showing the distribution of Dox@SiPINGs (Dox concentration of 5.0 μg mL^{-1}) in MCF-7/ADR cells before and after irradiation (808 nm, 0.5 W cm^{-2}, 10 min). The yellow color indicates the colocalization of the green channel (from OSiNDs) and red channel (from Dox) of Dox@SiPINGs. f) Schematic illustration showing that Dox@SiPINGs can bypass the drug efflux pump and realize nuclear drug delivery under the NIR light irradiation.

With their remarkable cellular uptake, the Dox@SiPINGs elicited significantly enhanced apoptosis toward MCF-7/ADR cells after irradiation by an 808 nm laser (0.5 W cm^{-2}) for 10 min (Figure 3c,d). In sharp contrast, the low uptake of free Dox resulted in its poor efficacy, which confirmed the robust resistance of MCF-7/ADR cells against free Dox. Typically, MCF-7/ADR cells preserved >80% of cell viability after treatment with 5.0 μg mL^{-1} Dox, while Dox@SiPINGs with the same Dox concentration were capable to effectively induce more than 60% cell apoptosis after irradiation. For MCF-7 cells, although the fluorescence intensity of the Dox channel in the Dox@SiPINGs-treated group was similar to that in free Dox-treated group (Figure S14b, Supporting Information), the anticancer efficacy of Dox@SiPINGs with irradiation was higher than that of free Dox as determined by MTT and apoptosis assay (Figure S14c,d, Supporting Information). This is probably because the fluorescence intensity of Dox was decreased in the nanogels (Figure S12b, Supporting Information) and the internalization

content of Dox@SiPINGs was much higher than that of free Dox at similar fluorescence intensities. Meanwhile, owing to their outstanding antileakage ability, Dox@SiPINGs presented much lower cytotoxicity to MCF-10A (a normal breast epithelial cell line) cells than free Dox (Figure S19, Supporting Information). To confirm the important photoactivatable role of ICG on the anticancer therapeutic outcome, Dox was encapsulated into the nanogels formed by OSiNDs and PEG–PLE (abbreviated as Dox@PSiNGs, with a hydrodynamic diameter of ≈58 nm, Figure S7d, Supporting Information) for comparison purposes. Although Dox@PSiNGs (without ICG) showed similar intracellular distribution with Dox@SiPINGs (Figure S20, Supporting Information), their incapability of photocontrollable drug release resulted in weak anticancer efficacy (Figure S21, Supporting Information). All these observations demonstrated the excellent performance of Dox@SiPINGs in killing tumor multidrug-resistant cells.

We further monitored the light-triggered drug release of Dox@SiPINGs in both MCF-7 and MCF-7/ADR cells by confocal microscopy (Figure 3e and Figure S14e, Supporting Information). Different from the distribution in the cytoplasm before irradiation, apparent intranuclear fluorescence signals were detected in the Dox@SiPINGs-treated cells after irradiation, illustrating the outstanding nucleus-targeted Dox delivery of the nanogels. Notably, the intranuclear fluorescence in the MCF-7/ADR cells exposed to Dox@SiPINGs and irradiation was mainly located in some spherical dots inside nuclei (Figure 3e), which were the nucleolar regions that play an important role in cell proliferation by producing ribosome and RNA.[25] Therefore, the dysfunction of nucleoli caused by the released Dox might be the possible mechanism leading to the death of MCF-7/ADR cells. Collectively, we could summarize the reversal of MDR as an NIR light-controllable process: In sharp contrast to the low intracellular uptake of free Dox, the Dox-encapsulated nanogels can evade the DETs on the plasma membrane via caveolin-, clathrin-, and macropinocytosis-dependent pathways and have significantly enhanced endocytosis in multidrug-resistant cells. The endocytosed Dox@SiPINGs are distributed in the cytoplasm with negligible cytotoxicity because of the excellent antileakage ability of the nanogels. Subsequently, activated by the NIR light, the Dox@SiPINGs are disassembled into small particles resulting from the photodegradation of ICG molecules. Meanwhile, a large number of Dox molecules are rapidly released from the nanogels, and occupy the cell nucleus even in the presence of DETs on nuclear membrane, which can be attributed to the following mechanisms: 1) The Dox release triggered by NIR light irradiation is so fast and massive that it exceeds the drug efflux rate of the DETs on the nuclear membrane, and 2) during the NIR light irradiation, the ICG molecules can induce the local hyperthermia and generate toxic reactive oxygen species (ROS), which may weaken the efflux ability of the DETs on the nuclear membrane. Finally, the intranuclear Dox can fully realize its therapeutic efficacy, achieving the circumvention of MDR (Figure 3f).

Motivated by the in vitro results, we then performed in vivo theranostic experiments using nude mice with subcutaneous xenograft tumors via the tail vein injection with Dox or Dox@SiPINGs. First, uterine cervical carcinoma U14 (a non-drug-resistant cell line) tumor models were established in mice for the following experiments. The fluorescence intensity of Dox@SiPINGs in the tumor regions (indicated by the white dotted circles) showed a continuous increase and reached a maximum at 24 h postinjection, whereas free Dox exhibited very weak fluorescence signals within the whole observation time period (**Figure 4**a,b). Such a direct fluorescence comparison verified the excellent tumor targeting ability and long tumor retention time of Dox@SiPINGs, which can be attributed to their proper size (≈40 nm, Figure S11b, Supporting Information) that endows them with excellent passive tumor targeting ability through the EPR effect, and the presence of PEG chains, which reduces the capture of NPs by reticuloendothelial system and prolongs the blood circulation time. Meanwhile, the nude mice intravenously (i.v.) injected with Dox or Dox@SiPINGs were sacrificed at 24 h postinjection. The ex vivo images and corresponding statistical results (Figure 4c,d) revealed that Dox@SiPINGs were mainly distributed in tumor with a partial deposition in liver, lung, and kidneys. In contrast, the free Dox group had much weaker fluorescence in tumor and relatively higher fluorescence in normal organs (except liver), which may lead to the lower antitumor efficacy of free Dox as compared with that of Dox@SiPINGs. Besides, we have also confirmed that Dox@SiPINGs had much lower long-term toxicity compared to free Dox by using normal liver L02 cells as a model (Figure S22, Supporting Information), possibly due to the low leakage rate of Dox@SiPINGs (Figure 1l).

Subsequently, inspired by the efficient in vitro therapeutic effect and the high tumor accumulation of Dox@SiPINGs, the in vivo tumor suppression capability of the nanogels was evaluated using both U14 and MCF-7/ADR tumor-bearing nude mice. On the basis of the aforementioned results, 24 h post-intravenous injection was chosen as an optimized time point for achieving sufficient tumor retention of Dox@SiPINGs for further tumor treatment. The tumor-bearing mice were randomly divided into six groups: physiological saline (control), SiPINGs, Dox, Dox@SiPINGs, SiPINGs + IR, and Dox@SiPINGs + IR, and the mice in the irradiation groups were exposed to an 808 nm laser (0.5 W cm^{-2}, 20 min) at 24 h postinjection. Different from the rapid tumor progression in the control group, both the U14 and MCF-7/ADR tumor growths of the mice in the Dox@SiPINGs-treated group after irradiation were remarkably inhibited during the total period of observation (Figure 4e and Figure S23a, Supporting Information). By comparison, free Dox treatment displayed negligible tumor elimination ability in MCF-7/ADR tumor-bearing mice and poor therapeutic performance for U14 tumor with a noticeable tumor regrowth after 10 days. As indicators of systemic toxicity, body weight and survival rate were monitored (Figure 4f,g and Figure S23b, Supporting Information). Free Dox caused severe weight loss of both U14 and MCF-7/ADR tumor-bearing mice, and even induced the death of mice in the U14 group, indicating the serious adverse effects of the drug. In contrast, the SiPINGs- and the Dox@SiPINGs-treated mice (with or without irradiation) had similar body weight curves as the control group. In particular, the combined treatment of Dox@SiPINGs and NIR light irradiation apparently prolonged host survival. These results further demonstrated the good phototherapeutic efficiency and favorable biocompatibility of Dox@SiPINGs.

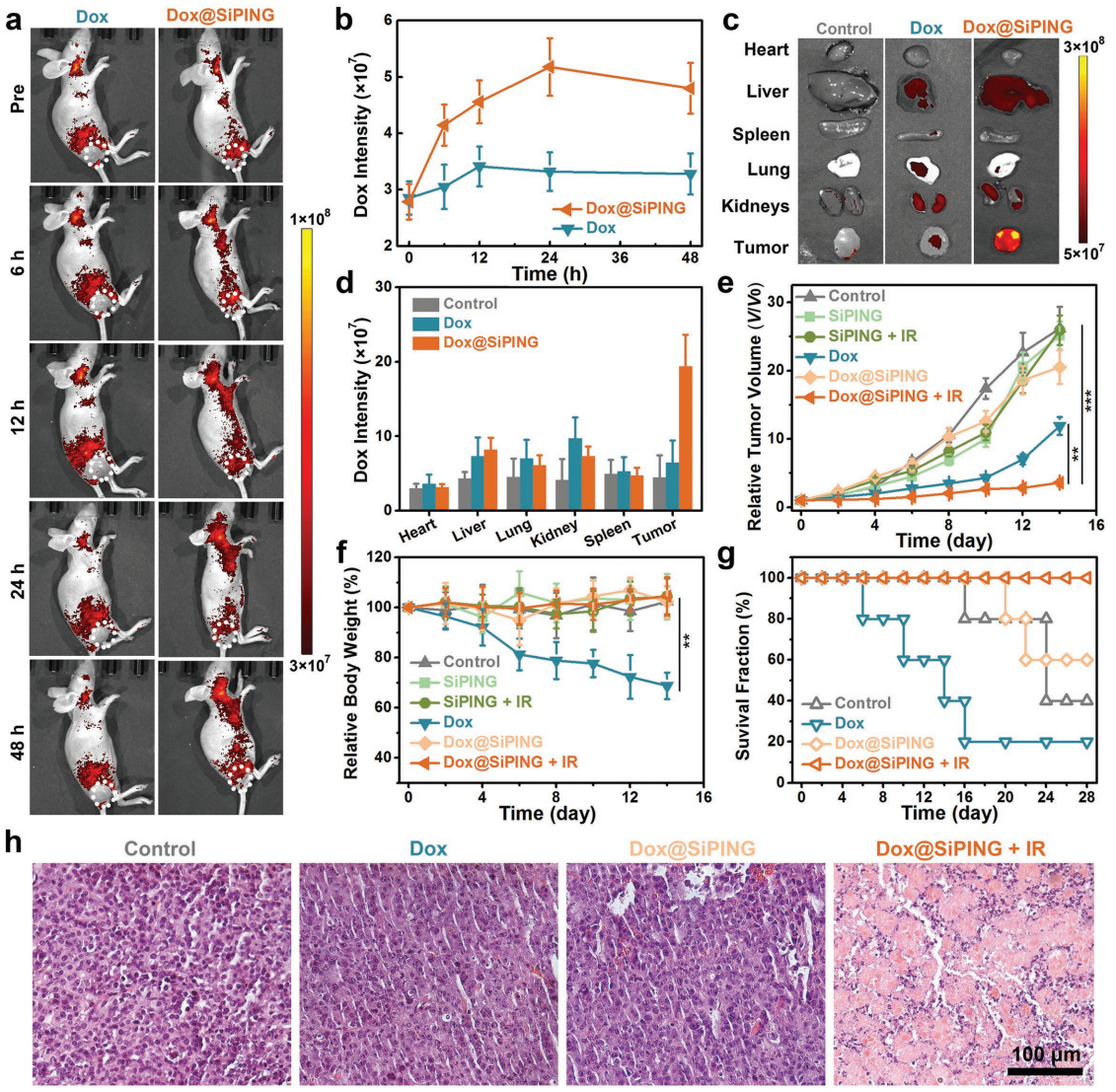

Figure 4. a) Time-dependent in vivo fluorescence images of U14 tumor-bearing mice after intravenous injection of Dox or Dox@SiPINGs, and b) the corresponding fluorescence intensities of Dox or Dox@SiPINGs within the U14 tumor areas at different time points. The white dotted circles in (a) indicate the positions of the tumor regions. c) Ex vivo fluorescence images of major organs and U14 tumor tissues excised from mice at 24 h post the intravenous injection of Dox or Dox@SiPINGs, and d) the corresponding fluorescence intensity results. e) U14 tumor growth curves of the mice after various treatments. $^{**}P < 0.01$, $^{***}P < 0.001$. f) Body weight changes of the U14 tumor-bearing mice after various treatments. $^{**}P < 0.01$. g) Survival rates of the mice after different treatments. h) H&E-stained U14 tumor slices from mice sacrificed on the 14th day after intravenous injection of physiological saline (control), Dox, Dox@SiPINGs, or Dox@SiPINGs + IR.

To further assess the antitumor activity and in vivo biocompatibility, the routine blood analysis, the evaluation of liver and kidney functions, and the hematoxylin and eosin (H&E) staining of tumor sections and major organs were performed for the mice sacrificed on the 14th day after various treatments. Unlike the compact tumor tissues of the physiological saline-(control), free Dox-, or Dox@SiPINGs-administrated groups, the Dox@SiPINGs with irradiation treatment caused a distinct drop in the number of tumor cells with significant nuclear condensation and fragmentation (Figure 4h), confirming their good tumor damaging effect. No abnormality from routine blood analysis and liver/kidney function assessment results and no tissue damage from the histopathologic results of major organs (including hearts, kidneys, livers, lungs, and spleen) were observed in the SiPINGs- and Dox@SiPINGs-treated groups (**Figure 5**a–c), which confirmed the excellent biosafety of the nanogels. In contrast, some notable alterations in the routine blood analysis data (such as the levels of white blood cells (WBCs), hemoglobin (HGB), hematocrit (HCT), platelet count (PLT), and plateletcrit (PCT)), subnormal liver function observed from the significantly elevated level of alanine aminotransferase (ALT), and partial damage of heart, kidneys, liver, and lung observed in the H&E-stained images were found in the Dox-treated group, indicating the systemic toxicity of free Dox. Collectively, the above results demonstrated that Dox@SiPINGs can be used as a robust and safe antitumor agent.

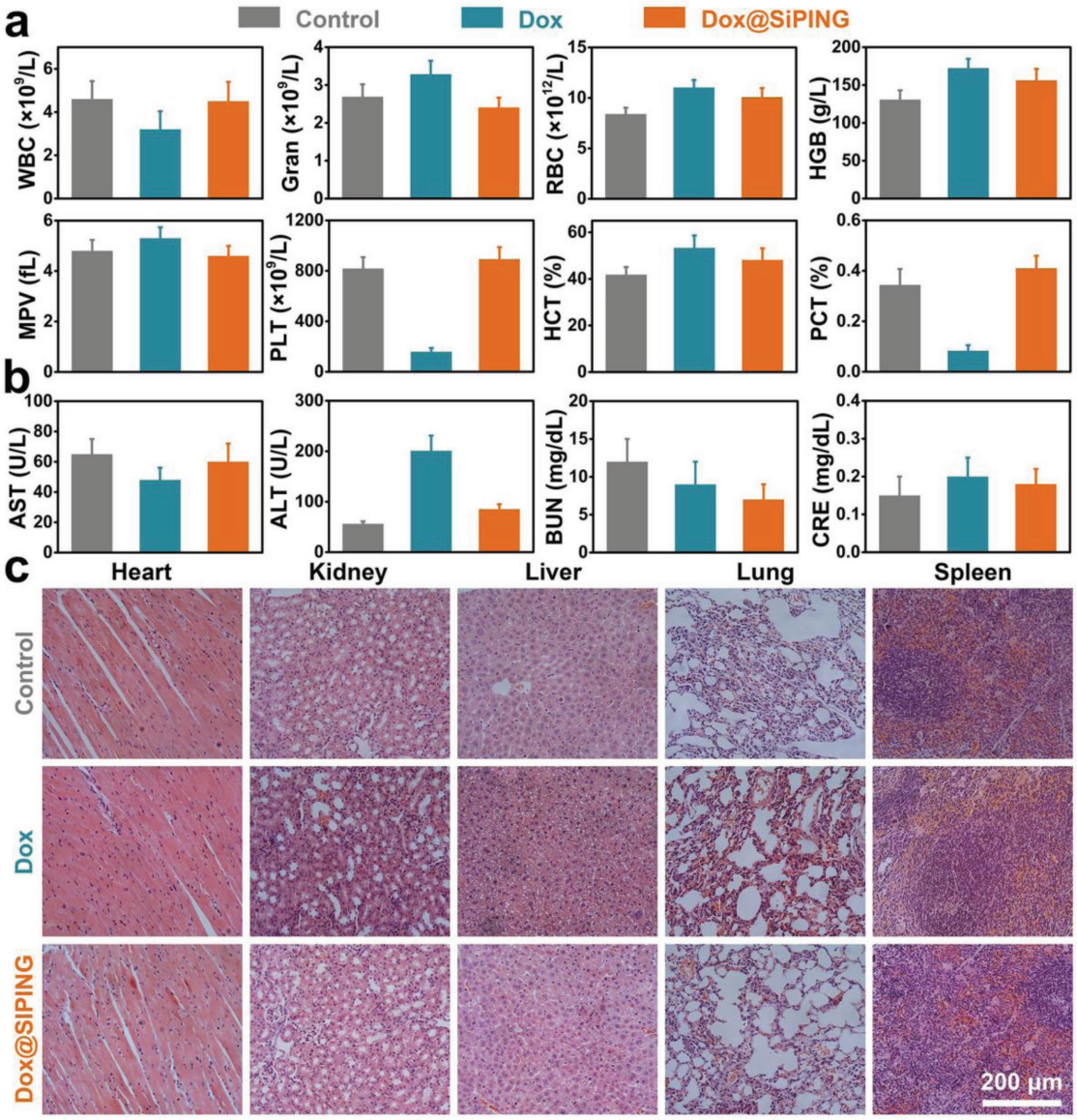

Figure 5. a) Routine blood analysis results of the mice collected on the 14th day after intravenous injection of physiological saline (control), Dox, or Dox@SiPINGs. The results show mean and standard deviation of white blood cells (WBCs), granulocyte (Gran), red blood cell (RBC), hemoglobin (HGB), mean platelet volume (MPV), platelets (PLT), hematocrit (HCT), and plateletcrit (PCT). b) Evaluation results of the liver and kidney functions of the mice collected on the 14th day after intravenous injection of physiological saline (control), Dox, or Dox@SiPINGs by examining the function-correlated biomarkers including the alanine aminotransferase (ALT), aspartate aminotransferase (AST), blood urea nitrogen (BUN), and creatinine (CRE). c) H&E staining assay results of major organs excised from mice treated with physiological saline (control), Dox, or Dox@SiPINGs.

3. Conclusion

In summary, the present work developed a simple strategy to construct supramolecular nanomedicines that realized remarkably enhanced cellular uptake and light-triggered nuclear drug influx in multidrug-resistant cells, thus overcoming two crucial issues induced by cancer MDR. As a proof of concept, photocontrollable "Trojan horse"-inspired nanogels (SiPINGs) with suitable size, proper surface coating, high drug encapsulation efficiency (≈99%) and loading efficiency (≈23.5%), passive tumor-targeting ability, significantly increased cellular endocytosis, and NIR light-triggerable nuclear delivery have been designed to combat multidrug-resistant cancers. The nanogels consist of three functional components: long-circulating PEG–PLE preventing the nanogels from being recognized by the DETs on plasma membrane for increasing tumor and cellular accumulation efficiencies of the nanogels, photodegradable ICG endowing the photoactivatable disassembly for photocontrollable drug release, and fluorescent OSiNDs as a bridge crosslinking the two other components and probe for bioimaging. The nanogels behaved as the "Trojan horses" that efficiently shielded and transported anticancer "soldiers" (Dox

molecules) into the cytoplasm of multidrug-resistant cells. Then, sufficient Dox molecules were rapidly released from the nanogels through an NIR light-triggered strategy and occupied the cell nucleus even in the presence of DETs on nuclear membrane. Therefore, excellent in vitro therapeutic effect against multidrug-resistant cells and significant in vivo tumor growth inhibition were achieved. Such a simple strategy to construct supramolecular nanomaterials for photocontrollable nuclear delivery of drugs will offer new opportunities to develop nanomedicines for circumvention of MDR.

4. Experimental Section

Synthesis of OSiNDs: The OSiNDs were synthesized as described in the previous work.[16] Briefly, 30 mg rose bengal (RB) was dissolved in 4 mL water, followed by the addition of 1 mL 3-[2-(2-aminoethylamino) ethylamino]propyl-trimethoxysilane (AEEA). Then, the mixture was transferred into a 10 mL Teflon-lined autoclave, which was sealed and maintained at a temperature of 160 °C for 4 h. After cooling down to the room temperature, the product was dialyzed (500 Da) to remove the residual reagents. The final sample was obtained through freeze drying.

Preparation of SiPINGs and Dox@SiPINGs: SiPINGs were prepared by sequentially adding the PEG–PLE (25 µL, 10 mg mL^{-1}), ICG (12.5 µL, 10 mg mL^{-1}), and OSiND (125 µL, 10 mg mL^{-1}) solutions to 837.5 µL deionized water. After vortexing for 30 s, the mixture was kept under ambient condition for 2 h to obtain SiPINGs. To prepare the Dox@SiPINGs, 25 µL PEG–PLE solution (10 mg mL^{-1}) and 12.5 µL ICG solution (10 mg mL^{-1}) were added to 712.5 µL deionized water, followed by the addition of 125 µL Dox solution (4 mg mL^{-1}) and 125 µL OSiND suspension (10 mg mL^{-1}). Then, the mixture was vortexed for 30 s and kept under ambient condition for 2 h. After centrifugation at 10 000 rpm for 5 min, the Dox encapsulation efficiency and loading efficiency were calculated by the following equations: Encapsulation efficiency = (1 − weight of unencapsulated Dox/total weight of Dox fed initially) × 100%; Loading efficiency = (total of Dox fed initially − weight of unencapsulated Dox)/total weight of nanogels × 100%.

NIR Light-Activatable Disassembly of SiPINGs Observed by Confocal Microscopy: MCF-7 or MCF-7/ADR cells were cultured in a 96-well plate (5×10^3 cells per well) overnight. Then, fresh cell culture media containing SiPINGs were used to replace the original culture media. The ICG concentrations of SiPINGs in MCF-7 and MCF-7/ADR cells were 0.13 and 1.25 µg mL^{-1}, respectively. After incubation for 24 h, the cells were stained with Hoechst 33342 for 10 min, followed by imaging under a confocal microscope (Leica, TCS SP8, Germany). Next, the cells were irradiated with an 808 nm laser (0.5 W cm^{-2}, 10 min) and incubated at 37 °C and 5% CO_2 for another 6 h. Finally, the disassembly of nanogels was observed using the confocal microscope. The excitation wavelengths of Hoechst 33342 and OSiNDs were 405 and 488 nm, respectively.

Cytotoxicity and Apoptosis Assay of SiPINGs, Dox, and Dox@SiPINGs with and without Irradiation: MCF-10A, MCF-7, or MCF-7/ADR cells were cultured in 96-well plates (5×10^3 cells per well) overnight and then incubated with various concentrations of SiPINGs, Dox, or Dox@SiPINGs for 24 h. Afterward, the cells were divided into two groups: irradiation group and nonirradiation group. The cells in the irradiation group were irradiated under an 808 nm laser (0.5 W cm^{-2}, 10 min), while the cells in the nonirradiation group were placed in the dark. Then, all the cells were cultured at 37 °C and 5% CO_2 for another 6 h. Finally, the cell viability was evaluated using MTT assay, and the cell apoptosis rate was analyzed by flow cytometry using an Annexin V-FITC/PI apoptosis detection kit (KeyGen Biotech, Nanjing, China). Each group had three parallel samples.

NIR Light-Controllable Dox Release of Dox@SiPINGs: MCF-7 or MCF-7/ADR cells were seeded in an 8-well plate (5×10^3 cells per well) overnight. Afterward, the original culture media were replaced by fresh culture media containing Dox@SiPINGs for 24 h. The Dox concentrations of Dox@SiPINGs in MCF-7 and MCF-7/ADR cells were 0.5 and 5.0 µg mL^{-1}, respectively. Then, the cells were divided into two groups (group I and II). The cells in group I were incubated in the dark for 6 h, while the cells in group II were irradiated with an 808 nm laser (0.5 W cm^{-2}) for 10 min, followed by incubation at 37 °C and 5% CO_2 for another 6 h. After that, the cells were incubated with Hoechst 33342 for 10 min to stain the cell nuclei and imaged under the confocal microscope. The excitation wavelengths of Hoechst 33342, OSiNDs, and Dox were 405, 488, and 552 nm, respectively.

Supporting Information

Supporting Information is available from the Wiley Online Library or from the author.

Acknowledgements

X.K.C and X.D.Z contributed equally to this work. This work was supported by the National Natural Science Foundation of China (Grant No. 21673037), the Natural Science Foundation of Jiangsu Province (Grant No. BK20170078), and the Scientific Research Foundation of Graduate School of Southeast University (Grant No. YBJJ1777). Z.C. thanks the University of Michigan for the support.

Conflict of Interest

The authors declare no conflict of interest.

Keywords

cancer theranostics, nuclear delivery, photocontrollable drug release, silicon-based nanomaterials, supramolecular assembly

Received: November 2, 2018
Revised: December 1, 2018
Published online: January 15, 2019

[1] a) L. M. Wang, Q. Sun, X. Wang, T. Wen, J. J. Yin, P. Y. Wang, R. Bai, X. Q. Zhang, L. H. Zhang, A. H. Lu, C. Y. Chen, *J. Am. Chem. Soc.* **2015**, *137*, 1947; b) L. P. Qiu, T. Chen, I. Ocsoy, E. Yasun, C. C. Wu, G. Z. Zhu, M. X. You, D. Han, J. H. Jiang, R. Q. Yu, W. H. Tan, *Nano Lett.* **2015**, *15*, 457; c) X. Wei, Y. Wang, X. Xiong, X. Guo, L. Zhang, X. B. Zhang, S. B. Zhou, *Adv. Funct. Mater.* **2016**, *26*, 8266; d) R. L. Zhang, S. Gao, Z. L. Wang, D. Han, L. Liu, Q. J. Ma, W. H. Tan, J. Tian, X. Y. Chen, *Adv. Funct. Mater.* **2017**, *27*, 1701027; e) Y. Yan, M. Bjornmalm, F. Caruso, *ACS Nano* **2013**, *7*, 9512.

[2] a) X. Wang, J. Li, Y. X. Wang, L. Koenig, A. Gjyrezi, P. Giannakakou, E. H. Shin, M. Tighiouart, Z. Chen, S. M. Nie, D. M. Shin, *ACS Nano* **2011**, *5*, 6184; b) R. R. Guo, Y. Tian, Y. J. Wang, W. L. Yang, *Adv. Funct. Mater.* **2017**, *27*, 1606398; c) C. B. He, K. D. Lu, D. M. Liu, W. B. Lin, *J. Am. Chem. Soc.* **2014**, *136*, 5181; d) Y. C. Li, X. H. Xu, X. Zhang, Y. K. Li, Z. J. Zhang, Z. W. Gu, *ACS Nano* **2017**, *11*, 416; e) N. H. Park, W. Cheng, F. Lai, C. Yang, P. F. de Sessions, B. Periaswamy, C. W. Chu, S. Bianco, S. Q. Liu, S. Venkataraman, Q. F. Chen, Y. Y. Yang, J. L. Hedrick, *J. Am. Chem. Soc.* **2018**, *140*, 4244; f) C. Yao, P. Y. Wang, X. M. Li, X. Y. Hu, J. L. Hou, L. Y. Wang, F. Zhang, *Adv. Mater.* **2016**, *28*, 9341; g) M. Z. Ye, Y. X. Han, J. B. Tang, Y. Piao, X. R. Liu, Z. X. Zhou, J. Q. Gao, J. H. Rao, Y. Q. Shen, *Adv. Mater.* **2017**, *29*, 1702342; h) R. X. Zhang, L. Y. Li, J. Li, Z. S. Xu, A. Z. Abbasi, L. Lin, M. A. Amini, W. Y. Weng, Y. Sun, A. M. Rauth, X. Y. Wu, *Adv. Funct. Mater.* **2017**, *27*, 1700804;

i) P. F. Zhao, W. M. Yin, A. H. Wu, Y. S. Tang, J. Y. Wang, Z. Z. Pan, T. T. Lin, M. Zhang, B. F. Chen, Y. F. Duan, Y. Z. Huang, *Adv. Funct. Mater.* **2017**, *27*, 1700403.

[3] Q. Wang, X. Y. Zhang, H. Z. Liao, Y. Sun, L. Ding, Y. W. Teng, W. H. Zhu, Z. R. Zhang, Y. R. Duan, *Adv. Funct. Mater.* **2018**, *28*, 1706124.

[4] a) Y. C. Zhou, F. T. Huang, Y. Yang, P. L. Wang, Z. Zhang, Y. N. Tang, Y. Q. Shen, K. Wang, *Small* **2018**, *14*, 1702446; b) J. Kim, Y. M. Lee, Y. Kang, W. J. Kim, *ACS Nano* **2014**, *8*, 9358.

[5] a) H. Meng, W. X. Mai, H. Y. Zhang, M. Xue, T. Xia, S. J. Lin, X. Wang, Y. Zhao, Z. X. Ji, J. I. Zink, A. E. Nel, *ACS Nano* **2013**, *7*, 994; b) Q. Q. Ni, F. W. Zhang, Y. L. Zhang, G. Z. Zhu, Z. Wang, Z. G. Teng, C. Y. Wang, B. C. Yung, G. Niu, G. M. Lu, L. J. Zhang, X. Y. Chen, *Adv. Mater.* **2018**, *30*, 1705737; c) H. J. Yu, Z. A. Xu, X. Z. Chen, L. L. Xu, Q. Yin, Z. W. Zhang, Y. P. Li, *Macromol. Biosci.* **2014**, *14*, 100; d) C. B. He, C. Poon, C. Chan, S. D. Yamada, W. B. Lin, *J. Am. Chem. Soc.* **2016**, *138*, 6010; e) X. B. Xiong, A. Lavasanifar, *ACS Nano* **2011**, *5*, 5202; f) M. Bai, M. Shen, Y. W. Teng, Y. Sun, F. Li, X. Y. Zhang, Y. Y. Xu, Y. R. Duan, L. F. Du, *Oncotarget* **2015**, *6*, 43779.

[6] M. H. Cho, S. Kim, J. H. Lee, T. H. Shin, D. Yoo, J. Cheon, *Nano Lett.* **2016**, *16*, 7455.

[7] a) Y. Gao, Y. Chen, X. F. Ji, X. Y. He, Q. Yin, Z. W. Zhang, J. L. Shi, Y. P. Li, *ACS Nano* **2011**, *5*, 9788; b) X. Guo, X. Wei, Y. T. Jing, S. B. Zhou, *Adv. Mater.* **2015**, *27*, 6450; c) Q. J. He, J. L. Shi, *Adv. Mater.* **2014**, *26*, 391; d) D. S. Ling, W. Park, S. J. Park, Y. Lu, K. S. Kim, M. J. Hackett, B. H. Kim, H. Yim, Y. S. Jeon, K. Na, T. Hyeon, *J. Am. Chem. Soc.* **2014**, *136*, 5647; e) H. J. Yu, Z. R. Cui, P. C. Yu, C. Y. Guo, B. Feng, T. Y. Jiang, S. L. Wang, Q. Yin, D. F. Zhong, X. L. Yang, Z. W. Zhang, Y. P. Li, *Adv. Funct. Mater.* **2015**, *25*, 2489; f) X. Ling, X. Chen, I. A. Riddell, W. Tao, J. Q. Wang, G. Hollett, S. J. Lippard, O. C. Farokhzad, J. J. Shi, J. Wu, *Nano Lett.* **2018**, *18*, 4618.

[8] a) X. Guo, L. Wang, K. Duval, J. Fan, S. B. Zhou, Z. Chen, *Adv. Mater.* **2018**, *30*, 1705436; b) Q. Q. Qu, Y. Wang, L. Zhang, X. B. Zhang, S. B. Zhou, *Small* **2016**, *12*, 1378.

[9] Y. Y. Zhou, L. X. Shi, Q. N. Li, H. Jiang, G. Lv, J. Zhao, C. H. Wu, M. Selke, X. M. Wang, *Biomaterials* **2010**, *31*, 4958.

[10] A. Calcabrini, S. Meschini, A. Stringaro, M. Cianfriglia, G. Arancia, A. Molinari, *Histochem. J.* **2000**, *32*, 599.

[11] a) M. Molina, M. Asadian-Birjand, J. Balach, J. Bergueiro, E. Miceli, M. Calderon, *Chem. Soc. Rev.* **2015**, *44*, 6161; b) R. Mo, T. Y. Jiang, R. DiSanto, W. Y. Tai, Z. Gu, *Nat. Commun.* **2014**, *5*, 3364; c) Y. T. Lim, S. M. Shim, Y. W. Noh, K. S. Lee, D. Y. Choi, H. Uyama, H. H. Bae, J. H. Kim, K. S. Hong, M. H. Sung, H. Poo, *Small* **2011**, *7*, 3281; d) W. Chen, Y. Zou, Z. Y. Zhong, R. Haag, *Small* **2017**, *13*, 1601997; e) K. I. Min, D. H. Kim, H. J. Lee, L. W. Lin, D. P. Kim, *Angew. Chem., Int. Ed.* **2018**, *57*, 5630; f) Y. S. Chen, S. J. Yoon, W. Frey, M. Dockery, S. Emelianov, *Nat. Commun.* **2017**, *8*, 15782; g) R. Kawasaki, Y. Sasaki, K. Katagiri, S. Mukai, S. Sawada, K. Akiyoshi, *Angew. Chem., Int. Ed.* **2016**, *55*, 11377; h) H. J. Kim, K. Y. Zhang, L. Moore, D. Hong, *ACS Nano* **2014**, *8*, 2998; i) M. Giulbudagian, G. Yealland, S. Honzke, A. Edlich, B. Geisendorfer, B. Kleuser, S. Hedtrich, M. Calderon, *Theranostics* **2018**, *8*, 450; j) H. B. Zhang, Y. Q. Zhu, L. L. Qu, H. Y. Wu, H. X. Kong, Z. Yang, D. Chen, E. Makila, J. Salonen, H. A. Santos, M. T. Hai, D. A. Weitz, *Nano Lett.* **2018**, *18*, 1448; k) X. D. Zhang, L. Y. Xia, X. K. Chen, Z. Chen, F. G. Wu, *Sci. China Mater.* **2017**, *60*, 487.

[12] a) F. F. Sahle, M. Giulbudagian, J. Bergueiro, J. Lademann, M. Calderon, *Nanoscale* **2017**, *9*, 172; b) B. Y. Shi, X. Du, J. Chen, L. B. Fu, M. Morsch, A. Lee, Y. Liu, N. Cole, R. Chung, *Small* **2017**, *13*, 1603966; c) F. Ding, Q. B. Mou, Y. Ma, G. F. Pan, Y. Y. Guo, G. S. Tong, C. H. J. Choi, X. Y. Zhu, C. Zhang, *Angew. Chem., Int. Ed.* **2018**, *57*, 3064; d) M. H. Xiong, Y. Bao, X. J. Du, Z. B. Tan, Q. Jiang, H. X. Wang, Y. H. Zhu, J. Wang, *ACS Nano* **2013**, *7*, 10636; e) M. H. Xiong, Y. Bao, X. Z. Yang, Y. C. Wang, B. L. Sun, J. Wang, *J. Am. Chem. Soc.* **2012**, *134*, 4355; f) Q. W. Zhu, X. J. Chen, X. Xu, Y. Zhang, C. Zhang, R. Mo, *Adv. Funct. Mater.* **2018**, *28*, 1707371.

[13] a) X. Wang, D. C. Niu, P. Li, Q. Wu, X. W. Bo, B. J. Liu, S. Bao, T. Su, H. X. Xu, Q. G. Wang, *ACS Nano* **2015**, *9*, 5646; b) M. Chan, J. Lux, T. Nishimura, K. Akiyoshi, A. Almutairi, *Biomacromolecules* **2015**, *16*, 2964; c) A. Yahia-Ammar, D. Sierra, F. Merola, N. Hildebrandt, X. Le Guevel, *ACS Nano* **2016**, *10*, 2591; d) C. Gota, K. Okabe, T. Funatsu, Y. Harada, S. Uchiyama, *J. Am. Chem. Soc.* **2009**, *131*, 2766.

[14] a) S. Y. Wang, G. Kim, Y. E. K. Lee, H. J. Hah, M. Ethirajan, R. K. Pandey, R. Kopelman, *ACS Nano* **2012**, *6*, 6843; b) S. Quan, Y. Wang, A. Zhou, P. Kumar, R. Narain, *Biomacromolecules* **2015**, *16*, 1978; c) Z. Khatun, M. Nurunnabi, M. Nafiujjaman, G. R. Reeck, H. A. Khan, K. J. Cho, Y. K. Lee, *Nanoscale* **2015**, *7*, 10680.

[15] K. Y. Win, S. S. Feng, *Biomaterials* **2005**, *26*, 2713.

[16] X. K. Chen, X. D. Zhang, L. Y. Xia, H. Y. Wang, Z. Chen, F. G. Wu, *Nano Lett.* **2018**, *18*, 1159.

[17] a) M. R. K. Ali, Y. Wu, D. Ghosh, B. H. Do, K. C. Chen, M. R. Dawson, N. Fang, T. A. Sulchek, M. A. El-Sayed, *ACS Nano* **2017**, *11*, 3716; b) Y. X. Zhu, H. R. Jia, G. Y. Pan, N. W. Ulrich, Z. Chen, F. G. Wu, *J. Am. Chem. Soc.* **2018**, *140*, 4062.

[18] X. K. Chen, X. D. Zhang, H. Y. Wang, Z. Chen, F. G. Wu, *Langmuir* **2016**, *32*, 10126.

[19] Y. H. Jiang, J. M. Fay, C. D. Poon, N. Vinod, Y. L. Zhao, K. Bullock, S. Qin, D. S. Manickam, X. Yi, W. A. Banks, A. V. Kabanov, *Adv. Funct. Mater.* **2018**, *28*, 1703982.

[20] a) X. D. Zhang, X. K. Chen, S. Q. Kai, H. Y. Wang, J. J. Yang, F. G. Wu, Z. Chen, *Anal. Chem.* **2015**, *87*, 3360; b) X. D. Zhang, X. K. Chen, J. J. Yang, H. R. Jia, Y. H. Li, Z. Chen, F. G. Wu, *Adv. Funct. Mater.* **2016**, *26*, 5958.

[21] Z. H. Sheng, D. H. Hu, M. M. Xue, M. He, P. Gong, L. T. Cai, *Nano-Micro Lett.* **2013**, *5*, 145.

[22] R. A. P. Harrison, S. E. Vickers, *J. Reprod. Fertil.* **1990**, *88*, 343.

[23] L. N. Shulman, C. M. Wagner, R. Barr, G. Lopes, G. Longo, J. Robertson, G. Forte, J. Torode, N. Magrini, *J. Clin. Oncol.* **2016**, *34*, 69.

[24] H. S. Yoo, E. A. Lee, T. G. Park, *J. Controlled Release* **2002**, *82*, 17.

[25] T. Pederson, *Nucleic Acids Res.* **1998**, *26*, 3871.